



Adsorption of PFOS onto graphite intercalated compound and analysis of degradation by-products during electro-chemical oxidation

Antoine P. Trzcinski^{a,*}, Kouji Harada^b

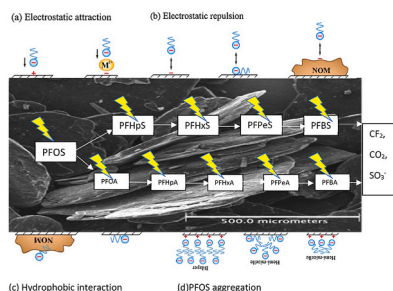
^a School of Agriculture and Environmental Science, University of Southern Queensland, West Street, 4350, Queensland, Australia

^b Department of Health and Environmental Sciences, Graduate School of Medicine, Kyoto University, Kyoto, 606-8501, Japan

HIGHLIGHTS

- Novel combined adsorption and electrochemical oxidation of PFOS was described.
- PFOS can be adsorbed with an adsorption capacity of 53.9 μg PFOS/g GIC.
- By-products include smaller chain perfluoroalkane sulfonates and carboxylic acids.
- Up to 99% PFOS removal after 40 min at a current of 0.5 A
- By-products can be also broken down but require longer time and at least 1.7 A

GRAPHICAL ABSTRACT



ARTICLE INFO

Handling Editor: E. Brillas

Keywords:

PFOS
Adsorption
Graphite intercalated compound
Electro-chemical oxidation

ABSTRACT

Perfluorooctane sulfonate (PFOS) is a highly recalcitrant perfluoro chemical belonging to the family of per- and polyfluoroalkyl substances (PFAS). Its adsorption and degradation was demonstrated in a novel PFAS remediation process involving the adsorption onto graphite intercalated compounds (GIC) and the electrochemical oxidation. The Langmuir type of adsorption was characterized by a loading capacity of 53.9 μg PFOS g^{-1} GIC and a second order kinetics (0.021 $\mu\text{g}^{-1} \text{min}^{-1}$). Up to 99% of PFOS was degraded in the process with a half-life of 15 min. The breakdown by-products included short chain perfluoroalkane sulfonates such as Perfluoroheptanesulfonate (PFHpS), Perfluorohexanesulfonate (PFHxS), Perfluoropentanesulfonate (PFPeS) and Perfluorobutanesulfonate (PFBS), but also short chain perfluoro carboxylic acids such as perfluorooctanoic acid (PFOA), perfluorohexanoic acid (PFHxA) and perfluorobutanoic acid (PFBA) indicating different degradation pathways. These by-products could also be broken down but the shorter the chain the slower the degradation rate. This novel combined adsorption and electrochemical process offers an alternative treatment for PFAS contaminated waters.

1. Introduction

Perfluorooctane sulfonate (PFOS) belongs to the family of per- and polyfluoroalkyl substances (PFAS) which have been widely used in

manufacturing processes and in firefighting foams used around air bases. This has caused major pollution of groundwater and surface water at concentration levels exceeding recommended doses. Due to its toxicity and strong carbon-fluorine bond, this chemical accumulates in

* Corresponding author.

E-mail address: antoine.trzcinski@usq.edu.au (A.P. Trzcinski).

<https://doi.org/10.1016/j.chemosphere.2023.138268>

Received 8 December 2022; Received in revised form 26 February 2023; Accepted 27 February 2023

Available online 2 March 2023

0045-6535/© 2023 Elsevier Ltd. All rights reserved.

the environment. The US environmental protection agency has recommended health advisory level of 70 ng L⁻¹ for total PFOS and perfluorooctanoic acid (PFOA) (EPA, 2016), but some states require a maximum PFOS level in drinking water at 13 ng L⁻¹ and 14 ng L⁻¹ for PFOA (Dadashi Firouzjaei et al., 2022). PFOS was found in Australian drinking water at a concentration of 16 ng L⁻¹ (Thompson et al., 2011), but concentration in groundwater around army bases have been reported at µg L⁻¹ levels. For instance, the average combined concentration of PFOS, PFOA and perfluorohexanesulfonic acid (PFHxS) in Oakey army site was 4.92 µg L⁻¹ (Leung et al., 2022).

Several technologies for the capture of PFOS and other PFAS exist such as reverse osmosis (Tang et al., 2006), activated carbon (Szabo et al., 2017) and polymeric resins (Kothawala et al., 2017), but PFAS are not destroyed by these methods, only transferred to another phase which creates a risk of re-pollution. Media such as activated carbon or resins must be incinerated or disposed of in landfills (Stoiber et al., 2020). Destruction technologies includes sonolysis using ultrasonication (Cheng et al., 2008), advanced oxidation processes (Vecitis et al., 2009), alkaline hydrolysis (Hao et al., 2021) and supercritical water oxidation (Pinkard et al., 2021). Ambaye et al. (2022) report that hydroxyl radicals alone produced during advanced oxidation processes have limited capacity to break the C–F bonds.

Complete cleavage of the C–F bond is required to avoid risks of re-contamination. Some technologies have been shown to breakdown PFOS, but some toxic short chain PFAS may still persist. Using supercritical water oxidation for 60 min, 70% PFOS destruction was achieved at 500 °C (Pinkard et al., 2021). These methods have a high cost prohibiting scale up of the technology. Compared to sonolysis (4000–11,000 kWh m⁻³) and ultrasonication (1475 kWh m⁻³), electrochemical oxidation (EO) has been reported to have much lower energy requirements (5–132 kWh m⁻³) (Sharma et al., 2022). Other advantages include normal temperature and pressure, possibility to scale up, higher removal efficiency and no requirement for external chemicals (Niu et al., 2012). In the electrochemical oxidation process, a small amount of electrolyte is required to improve the reaction and provide hydroxyl radicals and other oxidative species. Carter and Farrell (2008) have applied electrochemical oxidation using boron-doped diamond film electrodes and reported a half-life of 5.3 min at current density of 20 mA cm⁻². Some authors have used metal ions to supplement anodes and it has been shown to result in better performance. For instance, Ce-doped nanocrystalline PbO₂ resulted in the complete mineralization of C₄ to C₈ perfluorinated carboxylic acids (Niu et al., 2012). Using boron-doped diamond film electrodes, mineralization of perfluorobutane sulfonate (PFBS) is believed to occur through a combination of direct electron transfer and reactions with hydroxyl radicals (Liao and Farrell, 2009). However, the complexity of manufacturing and cost may hinder the implementation on large scale. EO can be achieved using either active or non-active electrode. Active electrodes such as Pt, Ti/Ru–IrO₂, and Ti/SnO₂–Sb/MnO₂, were found to be inefficient to mineralize PFAS, whereas up to 80% mineralization after 3 h was achieved using non-active electrodes such as tin oxide (SnO₂), lead dioxide (PbO₂), and boron-doped diamond (BDD) (Niu et al., 2013). This is because non-active electrodes have higher electron transfer ability, OH radicals generation and oxygen evolution potential (Niu et al., 2012). Possible limitations of these electrodes include low active surface area, release of toxic heavy metals in the water, fluorination of the electrode surface, fragile coating that can flake and the short service life of the substrate which means that these electrodes must be replaced after a short time (Niu et al., 2012). This also requires constant monitoring to know when changing the electrode is necessary.

Instead of using singular electrodes, it has been suggested to use a graphite intercalated compound (GIC) which can act as both an adsorbent and a conductive material, which can be regenerated in situ when placed between an anode and a cathode, thereby creating a combined adsorption and electrochemical oxidation (EO) process where the adsorbent is continuously regenerated. Such GIC adsorbent coupled

with EO has been proven successful to treat dissolved organic matter (Mohammed et al., 2011), greywater (Oki, 2015), azo-dye (Asghar et al., 2012), phenol (Hussain et al., 2013) and a wide range of microorganisms in water (Hussain et al., 2016b). Typical operating conditions include: 0.3% NaCl and HCl to pH < 2 in catholyte, current density of 20 mA cm⁻², duration of regeneration 20 min. Researchers reported that electrosorption or the enhanced adsorption in the presence of an electric current is an interesting option for PFAS removal. For instance, Li et al. (2011) reported that 94 times more PFOS and 150 times more PFOA were removed when 0.6 V was applied. This electrical current increases the charge on PFAS molecules which induces their mobility and improves their adsorption. Their LC-MS work also demonstrated that at 0.6 V no degradation of PFOA or PFOS took place and that the only removal mechanism was therefore adsorption. The aim of this paper was therefore to determine the capacity and kinetics of PFAS adsorption onto GIC, and once adsorbed, evaluate the electrochemical oxidation through the monitoring of breakdown by-products.

2. Methods and materials

2.1. Graphite intercalation compound

The adsorbent used in this study was an expandable graphite intercalation compound (GIC) in the form of flakes purchased from Sigma-Aldrich (P/N: 808121). A minimum of 75% of the flakes were larger than 300 µm. GIC is not porous and possess a low surface area of approximately 1 m² g⁻¹ (Hussain et al., 2016a). It is highly conductive with 0.8 S cm⁻¹ (Asghar et al., 2012).

2.2. PFOS

A technical mixture of heptadecafluorooctane sulfonic acid (C₈F₁₇KO₃S) was obtained from Fluka (P/N: 77282). A stock solution containing approximately 10 mg L⁻¹ was prepared for the experiments.

2.3. Batch adsorption tests

Batch adsorption tests were carried at 25 °C in 250 mL Erlenmeyer flasks to determine the adsorption capacity of graphite. A volume of 100 mL distilled water containing 1 g graphite was prepared and various volumes of stock solution were pipetted in each flask to achieve different initial concentrations. The flasks were placed on an orbital shaker at 150 rpm and samples were withdrawn over time until equilibrium was achieved. Samples were filtered using a 0.22 µm filter.

The effect on the adsorption intake of PFOS onto graphite for different parameters such as contact time, the amount of adsorbent, and initial concentration of PFOS were investigated. The amount of PFOS adsorbed at equilibrium, q_e (mg g⁻¹) was calculated as:

$$q_e = \frac{C_o - C_e}{M} \times V \quad (1)$$

where, C_o and C_e (mg L⁻¹) are the liquid-phase concentrations for initial sorbate and equilibrium respectively. V is the volume of the solution (L) and M is the mass of graphite used. Models such as Langmuir and Freundlich were fitted against the data according to previous literature (Mohammed et al., 2011). Kinetic models such as pseudo first and second order were fitted against the data according to previous literature (Trzcinski et al., 2011).

2.4. Electro-chemical reactor

The reactor used to study the combined adsorption and regeneration of graphite is shown in Fig. 1. It is made of Perspex acrylic plastic in a Y-shape. Its technical drawings were reported elsewhere (Mohammed et al., 2012).

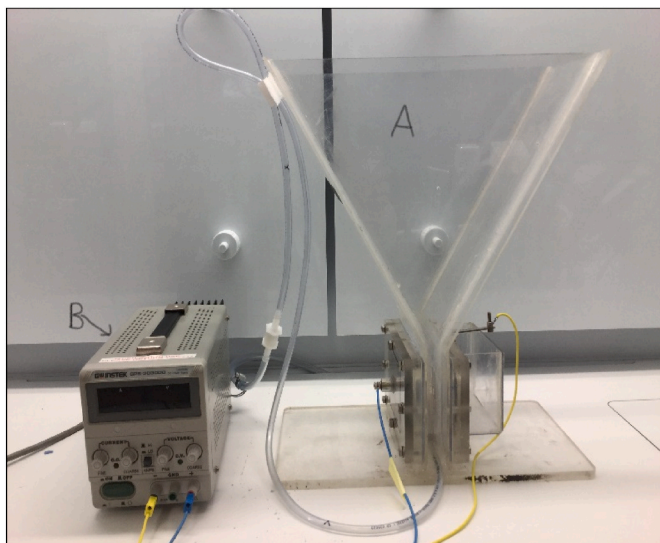


Fig. 1. (a) Electrochemical cell used in this study and (b) power supply unit (0–3 A and 0–30 V).

The top part is where adsorption takes place due to mixing caused by pumping air, while the bottom part is the regeneration zone between the cathode and anode. The anode was a graphite block with dimensions 100 by 70 mm and 5 mm thick. Its density was 1.72 g cm^{-3} , its specific resistance $8 \mu\Omega\text{m}$ and compressive strength 35 MPa (Grade PFR, Graphite Australia). The cathode was a perforated stainless steel with the same dimensions as the anode. The catholyte compartment is approximately 500 mL containing 3% NaCl and HCl to $\text{pH} < 2$ (unless mentioned otherwise). The active area of each electrode is 70 cm^2 . The distance between the anode and cathode is 6.3 cm and about 100 g of graphite was added to fill the regeneration zone (12 cm deep and 5 cm thick). The volume of the reactor chamber is about 6 L, but only 3 L was used for the experiments. The anodic and cathodic compartments were separated by a semipermeable Fumatech Anion Membrane (P/N: 5041682 purchased from FuelCellstore, USA) which in theory allows OH^- and chlorine anions to migrate across the membrane while excluding Na^+ and H^+ to avoid severe pH drop in the anodic compartment which was reported in past studies (Hussain et al., 2016b). The current was adjusted using a digital power supply (0–3 A, 0–30 V, GPS-3030DD, Instek, Taiwan). First, an air pump was used to keep the graphite in suspension and promote adsorption for 20 min, then the pump was stopped, and the graphite was allowed to settle in the regeneration zone for 2 min, after which the current was switched on for 10 min. For the experiments, three mL of the PFOS stock solution were injected in the 3 L reactor to give an initial concentration of approximately $10 \mu\text{g L}^{-1}$ in order to simulate typical groundwater contamination found in Australia. For instance, Oakey air base reported an average combined concentration of $4.92 \mu\text{g L}^{-1}$ for PFOS, PFOA and PFHxS (Leung et al., 2022).

2.5. Liquid-liquid extraction of PFOS

In a 2 mL Eppendorf centrifuge tube, a 200 μL sample was mixed with 200 μL of ion-pairing buffer (Tetrabutylammonium hydrogensulfate). 400 μL of methyl *tert*-butyl ether (MTBE) was then added to extract PFOS, mixed manually by shaking the tube, and then centrifuged at 5000 rpm for 3 min. The MTBE layer was then transferred carefully to a glass tube. The extraction, mixing and centrifuging steps were repeated using 200 μL MTBE. MTBE in glass tubes was then evaporated at 80°C under nitrogen stream. 20 μL of an internal standard (1 ng of 11H-perfluoroundecanoic acid) was then added and evaporated again before 200 μL of the derivatizing reagent Bis(4-*tert*-butylphenyl)-

iodonium hexafluorophosphate (BtBPI) in acetonitrile ($1\% \text{ w v}^{-1}$) was added, mixed by pipetting and then transferred to a GC-MS vial for analysis.

2.5. GC-MS analysis

A DB-5MS capillary column (30 m, 0.25 mm i.d., 0.25 μm film thickness) was used in an Agilent 6890 GC-5973MSD. The injection volume was 1 μL . The full conditions have been reported in a previous publication (Harada et al., 2020). The PFOS mixture contained 8 different isomers which were separated by the method. The 8 peaks were individually quantified, summed and reported as total PFOS. Three identical water samples spiked with PFOS were liquid-liquid extracted, injected on the GC-MS and the resulting average and standard deviation were found to be $10.92 \mu\text{g L}^{-1}$ and $0.68 \mu\text{g L}^{-1}$, respectively, corresponding to a coefficient of variation (CV) of 6.2%.

3. Results and discussion

3.1. Adsorption kinetics

The kinetics of PFOS adsorption onto graphite was studied at room temperature (25°C) in batch experiments using various initial PFOS concentrations in the range $14\text{--}1292 \mu\text{g L}^{-1}$ and a graphite concentration of 10 g L^{-1} . Fig. 2 shows the decrease in concentrations of PFOS following addition of graphite and it is clear that most of the removal occurred within 20 min of adsorption which is consistent with past studies on GIC (Brown et al., 2004; Hussain et al., 2015; Flores et al., 2018). This is much faster than adsorption onto porous activated carbon and anion-exchange resins which can take more than 50 h to reach equilibrium (Du et al., 2014).

Fig. 3 shows the PFOS loading onto the adsorbent which increased to a maximum of $65 \mu\text{g PFOS g}^{-1}$ GIC after 3 h at an initial PFOS concentration of $1162 \mu\text{g L}^{-1}$. As the PFOS concentration was increased from 14 to $1292 \mu\text{g L}^{-1}$, the percentage removal at equilibrium decreased from 68% to 42% whilst the PFOS loading on GIC increased from 0.964 to $53.9 \mu\text{g g}^{-1}$ (Fig. 3). The % removal efficiency shows a decreasing trend with an increasing concentration of PFOS which is in contrast with the adsorption capacity of the sorbent which increased with the increasing concentration. This is due to the increase in the mass transfer driving force and hence, the rate at which PFOS molecules pass from the bulk solution to the GIC (Caturla et al., 1998; Imagawa et al., 2000; Mondal et al., 2015).

High adsorption capacity values have been reported in the literature for PFOS adsorption onto porous adsorbents: 120 mg PFOS/g magnetic biochar (Hassan et al., 2022), $62 \text{ mg PFOS g}^{-1}$ granular activated carbon

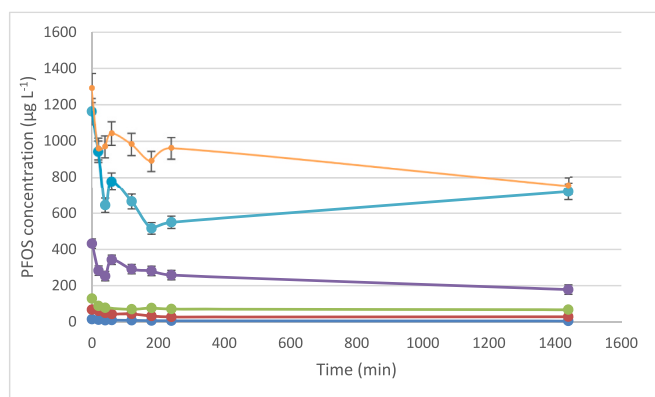


Fig. 2. Variation in the concentration of PFOS during the batch adsorption of PFOS on GIC (10 g L^{-1}) at 25°C for a range of initial concentrations (1292 , 1162 , 432 , 128 , 66.8 and $14.1 \mu\text{g L}^{-1}$). The error bars represent the coefficient of variation of 6.2% and were omitted when smaller than the marker.

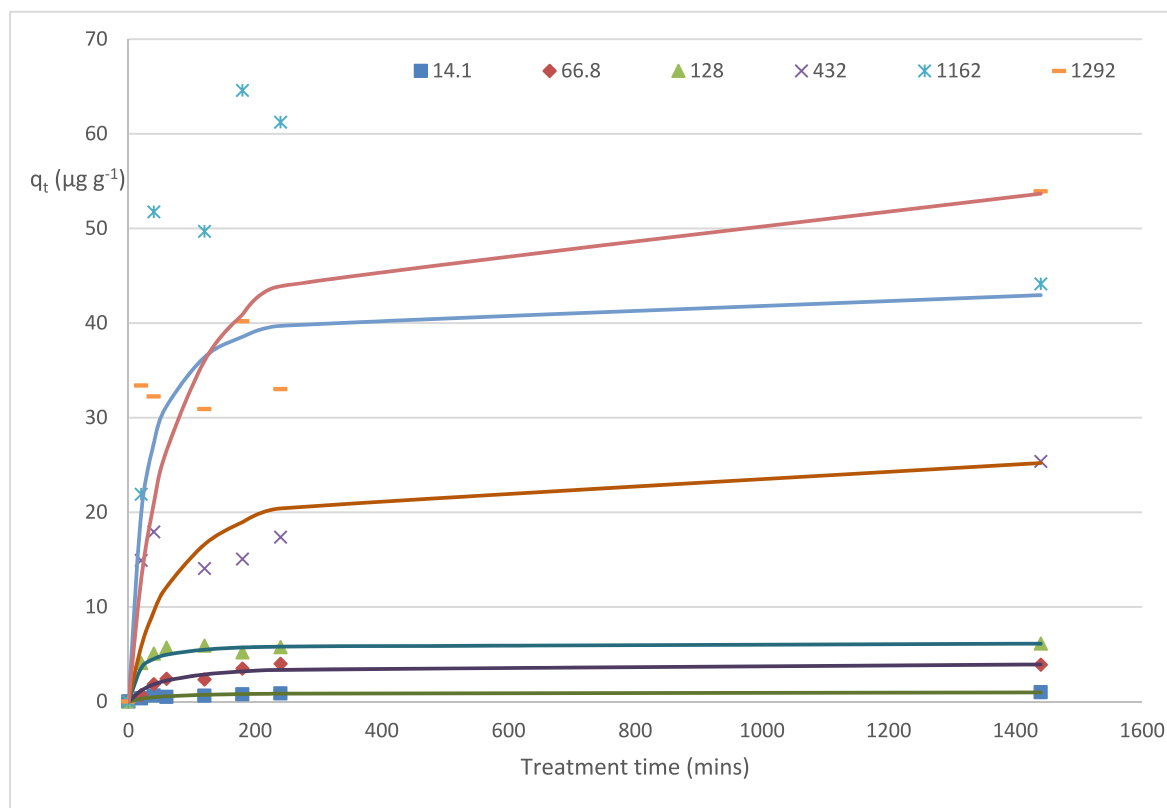


Fig. 3. Variation in the adsorbent loading of PFOS during batch adsorption on GIC calculated from data plotted in Fig. 2. The legend shows a range of initial concentrations (1292, 1162, 432, 128, 66.8 and 14.1 $\mu\text{g L}^{-1}$). The lines show the pseudo second order kinetic model fitted to the data.

(Zhang et al., 2021), 2390 mg g^{-1} ion exchange resin (Du et al., 2015). However, some studies have reported similar adsorption capacity of 28.4 $\mu\text{g PFOS g}^{-1}$ GAC and 80 $\mu\text{g PFOS g}^{-1}$ resins (Senevirathna et al., 2010).

In order to investigate the pseudo first and second kinetic model, the graphite loading (q_t) was calculated versus time for the data plotted in Fig. 2. Although the fit was not perfect, the second order kinetic model was better than the first order to describe the adsorption of PFOS onto GIC. The values of equilibrium loading obtained in the experiments ($q_{e, \text{exp}}$) are closer to the values obtained with the pseudo second-order model than those from the pseudo-first-order model. Fig. 3 shows the curve obtained from the pseudo second order model fitted to the data. The values for the kinetic constant k_2 , the calculated equilibrium loading and the coefficient of determination (R^2) obtained using the method of least squares fit are shown in Table 1.

3.2. Adsorption isotherms and mechanisms

The data was fitted to the Langmuir and Freundlich equations by linearizing the equations to determine the parameters for each model using the least squares method. The coefficient of determination R^2 shown in Table 1 indicates that the Langmuir model gave a better fit to the data than the Freundlich model suggesting a monolayer type of adsorption onto homogenous GIC where there is no interaction between adsorbed molecules and neighbouring adsorption sites. The Langmuir constant (b_L) of the adsorbent was 0.00214 (between 0 and 1) demonstrating that sorption was spontaneous and favourable. The value of n^{-1} in the Freundlich model was 0.9 indicating a desirable adsorption. The Freundlich constant (K_F) value was 0.1612 indicating a low affinity between sorbents and sorbates. The maximum sorption capacity was calculated as 53.9 $\mu\text{g g}^{-1}$ using the Langmuir isotherm model which is two to three orders of magnitude lower than that which can be achieved using activated carbons (Zhang et al., 2021).

Furthermore, Fig. 2 revealed an unstable adsorption suggesting that

Table 1

Kinetic rate constants for the adsorption of PFOS onto GIC (10 g L^{-1}), where q_{e1} and q_{e2} are the fitted equilibrium loadings for the first-order and second-order models, respectively. Langmuir and Freundlich isotherm constants for the adsorption of PFOS onto GIC.

Experimental data		First-order model			Second-order model		
C_0 ($\mu\text{g L}^{-1}$)	$q_{e, \text{exp}}$ ($\mu\text{g g}^{-1}$)	k_1 (min^{-1})	q_{e1} ($\mu\text{g g}^{-1}$)	R^2	k_2 ($\text{g } \mu\text{g}^{-1} \text{ min}^{-1}$)	q_{e2} ($\mu\text{g g}^{-1}$)	R^2
14	0.96	0.017	0.738	0.8921	0.0210	0.998	0.9989
67	3.89	0.0159	3.05	0.6821	0.0050	4.06	0.9957
128	6.12	0.0184	1.9	0.4002	0.0108	6.18	0.9996
432	25.4	0.0053	13.9	0.2497	0.0005	26.5	0.9906
1162	44.1	0.044	48.7	0.8283	0.0010	43.7	0.9962
1292	53.9	0.0062	30.6	0.3430	0.0003	56.2	0.9899
Langmuir	k_L ($\mu\text{g g}^{-1}$)	b_L ($\text{L } \mu\text{g}^{-1}$)	R^2	Freundlich	K_F ($\mu\text{g}^{1-1/n} \text{ L}^{1/n} \text{ g}^{-1}$)	n	R^2
	53.92	0.00214	0.9968		0.1612	1.108	0.981

some PFOS molecules were desorbing over time from the surface of the GIC adsorbent. The surface of the GIC adsorbent is non-porous so there is no pore filling mechanism involved. PFOS molecules were weakly adsorbed onto the adsorbent by van der Waals' attraction or other weak intermolecular forces. Mechanical stirring may have led to mild particle attrition and the release of weakly adsorbed PFOS from the surface of the particle electrode back into the bulk solution. PFOS is generally adsorbed through hydrophobic and electrostatic interaction (Elanchezhiyan et al., 2021). PFOS is in an anionic form at a wide pH range that can be sorbed through electrostatic interaction. However, the association of PFOS molecules with electrostatic interaction over the positive charge sites of the surface can be unsaturated to some extent because of repulsion behaviours among mobile and immobile PFOS molecules, resulting in some active sites remaining unsaturated. On the other side, two closely adsorbed molecules' hydrophobic tails could form hemimicelle because of the strong hydrophobic bond between the hydrophobic tails of PFOS molecules. The critical micelle concentration (CMC) of PFOS is $\sim 4573 \text{ mg L}^{-1}$ (Du et al., 2014; Hassan et al., 2020). For the formation of hemimicelle, the solution concentration should be about ~ 0.01 to 0.001% of the CMC (Du et al., 2014). In this isotherm study, the initial concentration of PFOS molecules exceeded the concentration of the critical hemimicelle. Thus, hemimicelle could have formed over the cationic active sites of GIC. Additionally, the bilayer formation of PFOS molecules could have formed onto hydrophobic tail-tail interaction (Hassan et al., 2022).

3.3. Electro-chemical oxidation of PFOS

3.3.1. Single PFOS spike

In this experiment, 3 mL of the PFOS stock solution was spiked in tap water, an initial sample was taken, then the water was poured in the reactor and the adsorption started by switching on the air pump. The aim of the experiment was to investigate the degradation of PFOS over successive adsorption and regeneration cycles and monitor the formation of PFOS degradation by-products.

After a spike at time 0, it can be seen from Fig. 4a that the PFOS concentration quickly decreases from an initial concentration of $13.3 \mu\text{g L}^{-1}$ to less than $0.85 \mu\text{g L}^{-1}$ after the first adsorption/regeneration cycle. The concentration progressively decreases further to less than $0.13 \mu\text{g L}^{-1}$ after 5 consecutive cycles ($>99\%$ removal). In comparison, the electron beam technology developed by Kowald et al. (2021) achieved only 16% PFOS removal in lab-spiked water and 41% in groundwater. Gu et al. (2016) achieved 98% PFOS decomposition after 30 min using hydrated electrons (e_{aq}^-) produced in a high photon flux UV/Sulfite system at pH 9.2 and 25°C . Intermediates included PFOA, PFHpA, PFHxA, PFPeA and PFBA and the mechanisms involved defluorination, desulfonation and centermost C-C bond scission.

Fig. 4b shows that PFOS was degraded to shorter chain PFOS such as perfluoroheptane sulfonate (PFHpS), PFHxS, perfluoropentane sulfonate (PFPeS) and PFBS. Smaller chain perfluoroalkane sulfonates with 3 and 2 carbons could not be detected using the method used in this study. After an initial increase during the first regeneration, it can be seen that the concentration of all four degradation by-products stabilized, but were not completely removed, except PFHpS.

PFHxS was found to be the dominant PFOS by-product but decreased from $3.6 \mu\text{g L}^{-1}$ to $0.758 \mu\text{g L}^{-1}$, demonstrating that it could also be adsorbed and broken down in the process to shorter chain by-products such as PFPeS and PFBS. PFPeS appeared after the first regeneration and its concentration stabilized between 0.08 and $0.037 \mu\text{g L}^{-1}$ without accumulating further or disappearing completely, indicating that it could be destroyed but not completely. Similarly, the 4 carbons by-product PFBS remained in water at concentrations ranging from $0.157 \mu\text{g L}^{-1}$ to $0.072 \mu\text{g L}^{-1}$, indicating that it was more difficult to adsorb and break down than the larger by-products. It was also observed that the main by product was PFHxS which was detected at a concentration 20 times greater than the other 3 by-products.

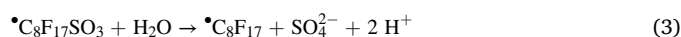
This batch experiment demonstrated that PFOS can be adsorbed onto GIC rapidly and it can be broken down into shorter PFOS by-products. Among these by-products, PFHpS could be completely removed after the second adsorption regeneration cycle, but PFHxS, PFPeS and PFBS could not be totally removed. At the end of the fifth cycle, PFHxS concentration was still $0.758 \mu\text{g L}^{-1}$ (88% removal), while PFPeS and PFBS concentrations were 37 ng L^{-1} (71.1% removal) and 72 ng L^{-1} (23% removal), respectively. In other words, the % removal decreased with smaller chain which can be due to lower adsorption capacity as smaller chain are more hydrophilic. A water sample was taken 12 h after the fifth cycle, and it was found that PFOS and its degradation by-products did not desorb into the water over time. At the end of the batch experiment, a sample of graphite was taken and extracted using the same procedure as for water samples. It was found that PFOS and PFOS degradation by-products were still adsorbed on graphite after 5 cycles suggesting that as PFOS and by-products were degraded, more adsorption sites became available on graphite following successive regeneration. Ultimately, the decrease in concentration in water indicates that PFOS and its by-products remains adsorbed on graphite until they were broken down.

Several mechanisms can explain the adsorption, removal and degradation of PFOS in the proposed process. When an external electrostatic field is imposed to GIC immersed in an aqueous electrolyte solution, the sides of the particle will gather positive or negative charge (Zhang et al., 2013). The charged PFOS anion is then attracted to the opposite charge on GIC flakes, resulting in the occurrence of electro-sorption. The combination of adsorption due to hydrophobicity of PFOS and electrosorption effectively promotes the removal of PFOS onto GIC. In our experiment, the pH of tap water was found to decrease from around 7 to between 2 and 3 after 3 to 5 cycles depending on the current applied. In the absence of alkalinity, the higher the current, the faster the pH drop due to a combination of diffusion of acid through the membrane and generation of acid at the anode (Mohammed et al., 2011). The use of a Fumatech anion membrane in these experiments did not prevent the migration of H^+ cations to the anodic compartment. Consequently, the acidic medium created conditions that allow a positive charge to be acquired by PFOS molecules which were then be attracted to negatively charged side of GIC flakes or onto the negatively charged electrode.

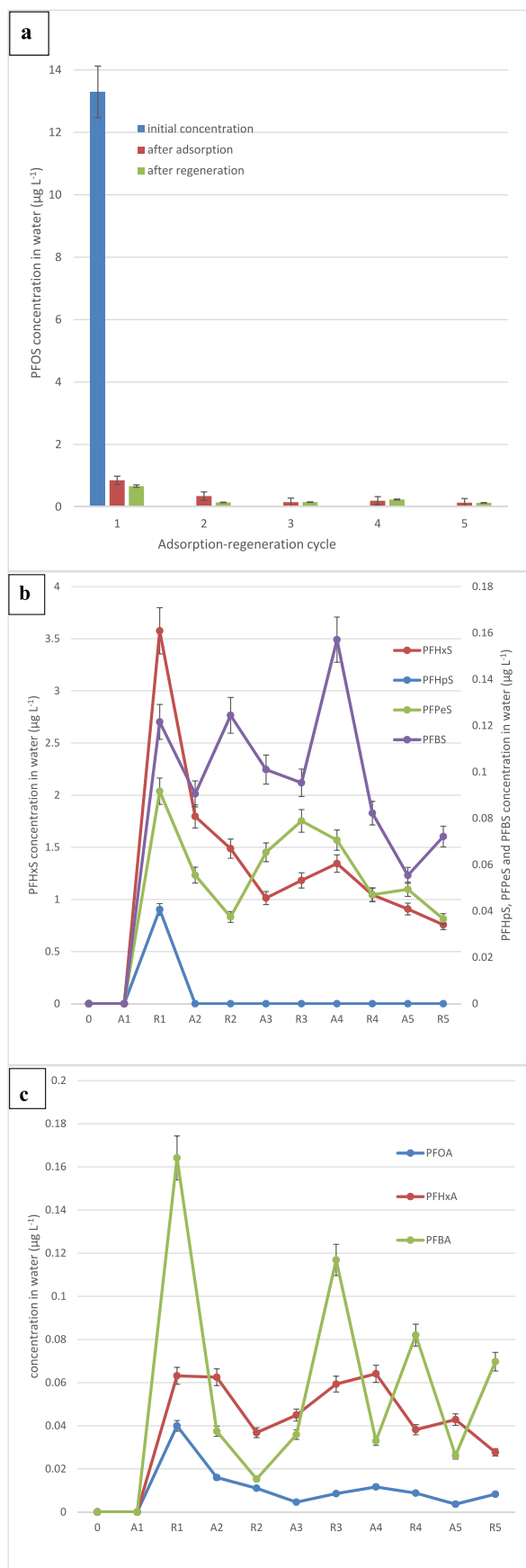
Furthermore, electrochemical oxidation processes generate hydroxyl radicals with a high oxidation potential, but Ambaye et al. (2022) report that hydroxyl radicals alone produced during advanced oxidation processes have limited capacity to break the C-F bonds. During electrochemical oxidation using electrodes, electron transfer reactions are involved. When the generation of e_{aq}^- is dominant compared to other reactive oxygen species such as $\cdot\text{OH}$, H_2O_2 , O_3 , $\cdot\text{O}_2^-$ and H_3O^+ , the degradation of PFOS via one-electron transfer mechanism become dominant due to e_{aq}^- high reduction potential of -2.9 V (Deng et al., 2021). When an electric field is applied, an electron from PFOS is initially transferred to the anode to form a PFOS radical according to the following reaction:



The radical would then decompose according to:



Subsequently, $\cdot\text{C}_8\text{F}_{17}$ will react with hydroxyl radicals to undergo a stepwise elimination of CF_2 subunits (Deng et al., 2021). According to that mechanism, after the C-S scission of $\cdot\text{C}_8\text{F}_{17}\text{SO}_3^-$, it will decompose into C_8F_{17} followed by the production of $\text{C}_8\text{F}_{17}\text{OH}$, which is subsequently converted to PFOA (Gu et al., 2016). On the other hand, $\cdot\text{C}_8\text{F}_{17}$ may be formed in the desulfonation reaction, before being transformed to PFOA (Bentel et al., 2019). It can be seen in Fig. 4c that PFOA was indeed produced from the degradation of PFOS which confirms the degradation pathway during the combined adsorption and electrochemical oxidation process using GIC. In the first pathway, $\cdot\text{C}_8\text{F}_{17}$ will



(caption on next column)

Fig. 4. (a). Evolution of PFOS concentration following one spike of concentrated PFOS stock solution into the electrochemical reactor. Each cycle comprises 20 min of adsorption and 10 min of regeneration at 0.489–0.544 A and 30.6 V. A stands for adsorption and R stands for regeneration. The error bars represent the coefficient of variation of 6.2%. (b) Evolution of smaller chain perfluoroalkane sulfonates after a single PFOS spike at time 0. (c) Evolution of smaller chain perfluoro carboxylic acids after a single PFOS spike at time 0.

react with hydroxyl radicals to yield $\text{C}_8\text{F}_{17}\text{OH}$ which will then decompose into HF and $\text{C}_7\text{F}_{15}\text{CFO}$. The latter will then hydrolyze into $\text{C}_7\text{F}_{15}\text{COO}^-$, HF and H^+ . This leaves us with a carboxylic acid which will undergo successive steps: firstly, Kolbe decarboxylation (releasing $-\text{CO}_2$), radical reaction involving $\cdot\text{OH}$, intramolecular rearrangement (releasing $-\text{HF}$) and hydrolysis (releasing $-\text{HF}$) to get rid of one CF_2 unit (Niu et al., 2012). The same cycle is then repeated until PFCAs are finally mineralized to CO_2 and HF. In the second pathway with an excess of oxygen, the radical $\text{C}_8\text{F}_{17}\text{OO}\cdot$ is produced. It can react with other radicals with a general form of $\text{RFOO}\cdot$ to yield $\text{C}_8\text{F}_{17}\text{O}\cdot$, $\text{RFO}\cdot$ and O_2 . $\text{C}_8\text{F}_{17}\text{O}\cdot$ will then decompose into C_7F_{15} and COF_2 . The latter will hydrolyze into CO_2 and HF. The radical $\text{C}_7\text{F}_{15}\cdot$ will then undergo the same pathways until complete defluorination.

As it can be seen from Fig. 4c, PFOA was broken down into perfluoroheptanoic acid (PFHpA), which was in turn broken down to perfluorohexanoic acid (PFHxA), perfluoropentanoic acid (PFPeA), and perfluorobutanoic acid (PFBA). Smaller chain perfluorocarboxylic acids (PFCAs) (less than 4 carbons) could not be detected using the method used in this study. PFOA was detected at 40 ng L^{-1} , then decreased to below 10 ng L^{-1} (79% removal) confirming that it could be broken down during the process. PFHpA and PFPeA were below detection limit ($\sim 10 \text{ ng L}^{-1}$) indicating that it could be readily degraded to PFHxA and PFBA, respectively. PFHxA and PFBA were detected at 63 ng L^{-1} and 164 ng L^{-1} , respectively, and decreased slowly to 28 ng L^{-1} (56% removal) and 70 ng L^{-1} (57.5% removal) over 5 cycles, indicating that even numbered short chain perfluoro carboxylic acids destruction was slower or limited by the availability of adsorption sites or low adsorbability. These results show that the electrochemical oxidation process using GIC was able to both break C–S bonds to lead to PFOA (Fig. 4c) as well as C–F bonds to lead to sulfonated by-products (Fig. 4b). The presence of PFOA and PFOA by-products confirmed the pathway described in the literature and suggest that hydrated electrons (e_{aq}^-) were also produced in the process leading to defluorination, desulfonation, and centermost C–C bond scission (Gu et al., 2016). Based on the higher concentration of PFHxS, it appears that the dominant pathway in the process was the shortening of PFOS molecules leading to smaller chain perfluoroalkanesulfonates.

These results contradict most AOP degradation studies that reported short chain (C_4 – C_7) PFCAs as the main by-products from PFOS treatment, but not shorter chain perfluoroalkanesulfonates (PFSAs). During plasma treatment of PFAS contaminated water, Singh et al. (2019) reported that PFOA, PFHxS and PFBS can all be by-products of PFOS degradation which is consistent with our work where short chain PFHpS, PFHxS, PFPeS and PFBS were detected in Fig. 4b and PFOA and its by-products were detected in Fig. 4c. Plasma technology works by producing highly reactive species such as $\cdot\text{OH}$, O , $\text{H}\cdot$, $\text{HO}_2\cdot$, $\text{O}_2^-\cdot$, H_2 , O_2 , H_2O_2 , and aqueous electrons (e_{aq}^-) using an electric field and the similarity of Singh et al. results with our suggested that the electrooxidation method using GIC as adsorbent might be comparable to a milder plasma technology operating at 30 V instead of 30 kV. Singh et al. (2019) further explained that PFHxS and PFBS may be formed by the reactions of $\text{SO}_3^-\cdot$ with $\cdot\text{C}_6\text{F}_{13}$ and $\cdot\text{C}_4\text{F}_9$, respectively. They note that perfluoroheptanesulfonate (PFHpS) or perfluoropentanesulfonate (PFPeS) were not measured in their work due to a lack of analytical standards, but they said it is likely that they would also have formed following the proposed degradation pathway. The presence of PFHpS and PFPeS in our work suggests that this is correct. The work by (Rodriguez-Freire et al., 2015) on sonolysis of PFOS also suggests that cleavage of the sulfonic

head does not take place and that shorter chain perfluoroalkyl sulfonic acids are formed as intermediates.

In our experiment, the successive adsorption and regeneration steps were carried out in the same batch of water and as result, the pH of tap water was found to decrease from around 7 to between 2 and 3 after 3 to 5 cycles depending on the current and voltage applied. In the absence of alkalinity, the higher the current, the faster the pH drop due to a combination of diffusion of acid through the membrane and generation of acid at the anode (Mohammed et al., 2011). Under acidic (due to acid in the catholyte) and oxygen rich conditions (due to air sparging used for mixing), it is also possible the traditional pathways documented in the literature were affected and that fluorine atoms were replaced by hydrogen atoms following hydrofluorination reactions. This substitution reaction would occur at the location next to the sulfonic headgroup, but this normally happens during photochemical and thermal degradation of PFOS and not during electrochemical oxidation (Deng et al., 2021). The presence of chlorine in the catholyte solution in the form of NaCl and HCl may also lead to additional indirect oxidation that involved electrogenerated active chlorine species such as Cl_2 , HOCl and OCl^- .

3.3.2. Second single PFOS spike

A second experiment was then conducted at a higher current of 1.768 A and the decrease in PFOS concentration is shown in Fig. 5a. Again, the by-products included shorter chain perfluoroalkane sulfonates (Fig. 5b), as well as PFCAs (Fig. 5c).

During this second batch experiment, PFOS concentration decreased to $2.87 \mu\text{g L}^{-1}$ after the first adsorption, and then to $1.525 \mu\text{g L}^{-1}$ after the first regeneration indicating that the regeneration at 1.768 A was oxidizing adsorbed PFOS molecules and was regenerating some active adsorption sites on GIC. The decrease after regeneration can also be seen in the second cycle. The decrease after the first cycle was not as sharp as it was observed in the previous batch experiment presumably because more graphite adsorption sites were saturated after the first batch experiment. After 4 cycles, the concentration was still $0.136 \mu\text{g L}^{-1}$. The decrease in degradation by-products in Fig. 5b indicates that PFOS was continuously broken down into shorter perfluorosulfonates and these were continuously adsorbed onto graphite or further broken down. The initial concentrations of PFOS degradation by-products were not zero due to residual by-products from the first experiment (Fig. 4a, b and c) still being present on the GIC as it was not possible to replace it with fresh GIC. Only PFHpS was non detectable after the second cycle. It was observed again that 3 degradation by-products PFHxS, PFPeS and PFBS could be broken down during the process, but were still detected at concentrations of $0.988 \mu\text{g L}^{-1}$, 0.054 and $0.042 \mu\text{g L}^{-1}$, respectively. Given the higher concentration of PFHxS during the degradation process, it can be said that the degradation of PFHxS was the rate-limiting step during the electro-chemical oxidation of PFOS on GIC.

Although PFOS, PFHpS and PFHxS could be broken down at a current of about 0.5 A (current density of 7.8 mA cm^{-2}), it is clear from Fig. 5b that a higher current of 1.768 A (current density of 25 mA cm^{-2}) was much more effective especially for PFPeS (71% removal) and PFBS (74% removal) due to higher electrons transfer rates, hydroxyl radicals production and possibly other chlorine-based radicals generation. Fig. 5c shows the evolution of PFOA and shorter chain PFHxA and PFBA and although PFOA could be broken down to less than 18 ng L^{-1} (71% removal), the degradation of PFHxA (36% removal) and PFBA (−2% removal) was not significant even at a higher current density. In comparison, the removal percentage of PFOS, PFHpS, PFHxS, PFPeS, PFBS, PFOA, PFHxA and PFBA were 98.97%, >93.5%, 85.7%, 71.2%, 74.7%, 71.1%, 36.4% and −2.6%, respectively, after 4 cycles of 20 min of adsorption and 10 min of regeneration (total time of 120 min of combined adsorption and electrochemical oxidation). In comparison, Singh et al. (2021) developed an enhanced contact plasma reactor and tested its performance on landfill leachate containing a range of PFAS including PFOA and PFOS, which was about 2000–3000 ng L^{-1} in concentration. With a treatment volume of 500 mL and applied voltage

of 30 kV, 90% of PFOA and PFOS were removed in 10 min of operation. In this experiment, the reaction kinetics followed a first-order for PFOS and the by-products, and the parameters including rate constants (k), half-lives ($t_{1/2}$), and R^2 determined using linear regression are summarized in Table 2.

As shown in Table 2, the k values are following this order: $k_{\text{PFOS}} \approx 1.06k_{\text{PFHpS}} \approx 2.2k_{\text{PFHxS}} \approx 3.2k_{\text{PFPeS}} \approx 3.32k_{\text{PFOA}} \approx 3.98k_{\text{PFBS}}$. According to the k values, the degradation $t_{1/2}$ values were calculated as 15, 16, 33, 49, 50 and 60 min for PFOS, PFHpS, PFHxS, PFPeS, PFOA and PFBS, respectively. The results confirmed that perfluoroalkane sulfonate and carboxylic acids chain length have a significant effect on the observed kinetics. In agreement with previous results, the degradation rates for PFOX ($X = \text{S}$ or A) are faster than their corresponding PFBX ($X = \text{S}$ or A) (Niu et al., 2012). Niu et al. (2012) achieved 96.7% PFOA removal using a Ce-doped modified porous nanocrystalline PbO_2 film electrode. At an initial concentration of 100 mg L^{-1} , the kinetics also followed a first order with $k = 3.7 \times 10^{-2} \text{ min}^{-1}$ and $t_{1/2} = 18.7 \text{ min}$. These results suggest that the affinity of PFOA with the PbO_2 film electrode was much better than with GIC used in this study.

Despite not being able to completely remove PFOS and its by-products, the process has been shown to remove them quickly below the health-based guidelines values recommended by the Australian government (NHMRC, 2022) which stipulates a total sum for PFOS and PFHxS of $2 \mu\text{g L}^{-1}$ and $10 \mu\text{g L}^{-1}$ for PFOA in recreational waters. It can be seen that three cycles of adsorption/regeneration would result in less than $2 \mu\text{g L}^{-1}$ for total PFOS and PFHxS. Unfortunately, the process would not be able to produce drinking water for which the health based guideline value is $0.07 \mu\text{g L}^{-1}$ (NHMRC, 2022). The process showed however better efficiency towards PFOS, but is less efficient towards PFOA which would require an adsorbent with a better affinity.

3.3.3. Single PFOS spike after each cycle

During this experiment, 3 mL of the PFOS stock solution was spiked after each adsorption/regeneration cycle as indicated by the red arrows in Supplementary material S1. This was done to investigate the possible accumulation of PFOS or its degradation by-products in water.

This experiment was initially conducted using 1.769 A and 19.7 V and it can be seen that PFOS concentration was below 95 ng L^{-1} after 2 cycles (99.6% removal) demonstrating the efficiency of the process to quickly adsorb and degrade PFOS. It is the electrical charge that drives the electrochemical regeneration, it is therefore important to maintain a constant current during the tests. The degradation of PFOS was demonstrated by the presence of short chain PFOS such as PFHxS, PFPeS and PFBS. After the second cycle, the current was reduced to 1 A in an attempt to reduce the production of chlorine gas and interestingly this led to a gradual accumulation of PFOS to $0.6 \mu\text{g L}^{-1}$. This is still a remarkable 99% PFOS removal after 5 spikes and 5 cycles consecutive adsorption regeneration cycles. This indicates that 1 A and 14 V was insufficient to fully restore the adsorption sites on graphite. However, given the small increase in PFOS concentration after 5 spikes (equivalent to a cumulative total concentration of $50\text{--}60 \mu\text{g L}^{-1}$), 99% of PFOS was either decomposed or adsorbed during the process.

More significantly, the short-chain sulfonates started to accumulate as well under these conditions until the end of the experiment showing that the adsorbed PFOS was broken down into smaller fragments. This accumulation after the second cycle using a regeneration amperage of 1 A is a sign that the current was not sufficient to oxidize all the molecules or produce sufficient hydroxyl radicals to attack all the molecules. As the molecules were not broken down sufficiently fast, the adsorption sites on the graphite became saturated and this led to an increase in the concentration in the water as it can be seen in Fig. S2. In addition, given the relative small increase in PFOS concentration (from 0.176 to $0.6 \mu\text{g L}^{-1}$) compared to the increase in PFHxS (from 0.935 to $6 \mu\text{g L}^{-1}$) during the last 3 cycles, it can be concluded that PFHxS was more recalcitrant to electrochemical oxidation whether it was by electron transfer, hydroxyl radical attacks or by electrochlorination confirming that the breakdown

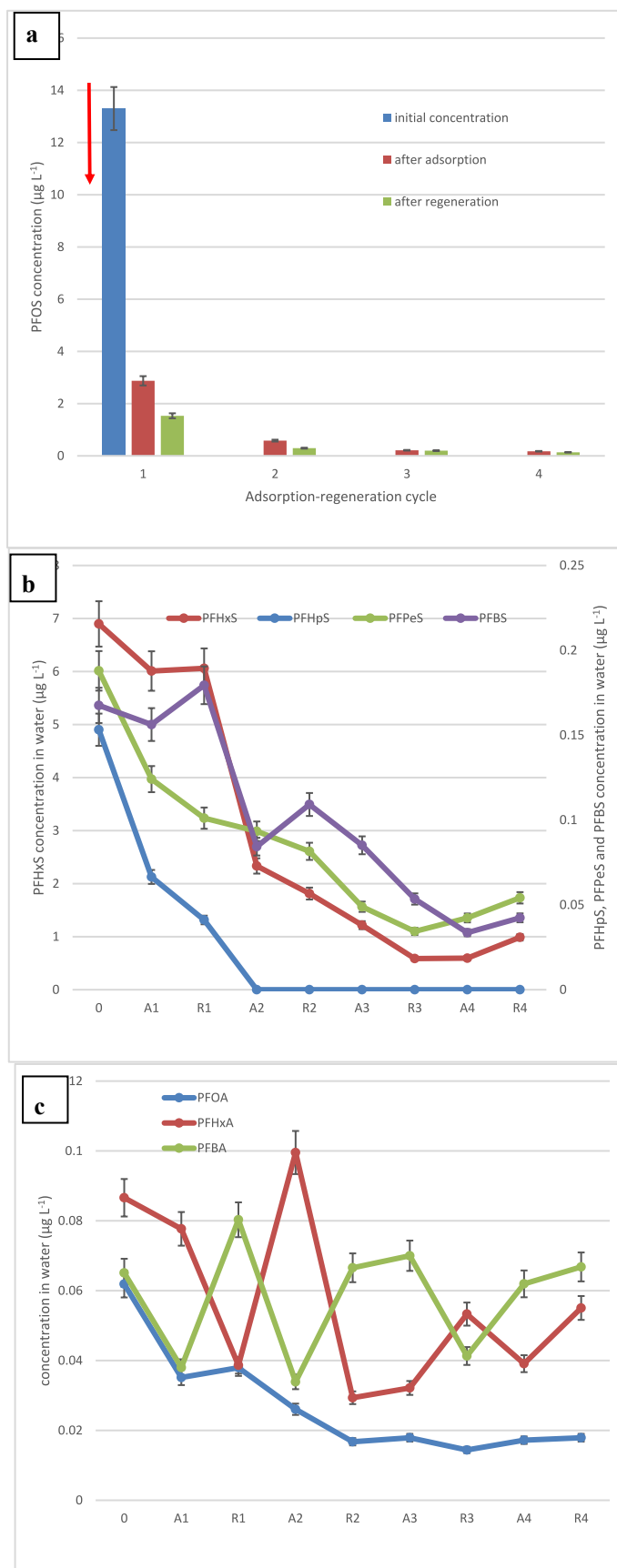


Fig. 5. (a). Evolution of PFOS concentration following one spike of concentrated PFOS stock solution (red arrow) into the electrochemical reactor. Each cycle comprised 20 min of adsorption and 10 min of regeneration at 1.768 A (Constant current). The error bars represent a coefficient of variation of 6.2%. (b) Evolution of short chain perfluoroalkane sulfonates after a single PFOS spike at time 0. (c) Evolution of PFOA, PFHxA and PFBA after a single PFOS spike at time 0.

Table 2

Efficiency and kinetics for PFOS removal and its degradation by-products during the combined adsorption and electrochemical oxidation process.

	Removal (%)	1st order rate constant (k_1 in min^{-1})	Half-life (min)	R^2
PFOS	98.97	0.0458	15	0.9584
PFHpS	>93.5	0.0432	16	0.9995
PFHxS	85.7	0.0208	33	0.9534
PFPeS	71.2	0.0142	49	0.9517
PFBS	74.7	0.0115	60	0.9327
PFOA	71.1	0.0138	50	0.9347
PFHxA	36.4	–	–	–
PFBA	–2.6	–	–	–

of PFHxS is the rate limiting step in the process. It also shows that although it is fairly easy to break down PFOS at a current of 0.5 A (Fig. 4a), a current of 1.7 A is required to break down PFHxS (fig. 5b and S2). Similarly, PFPeS and PFBS increased from 67.1 ng L^{-1} to 418 ng L^{-1} and 93.8–553 ng L^{-1} , respectively, despite some reduction observed after the application of the current at R3 and R4 (Fig. S2). This indicates that 10 min regeneration was not sufficient to fully oxidize the by-products and regenerate the initial adsorption capacity of GIC. Similarly to perfluoroalkane sulfonates (Fig. S2), PFOA, PFHxA and PFBA concentrations were found to increase several folds from 7.4 ng L^{-1} to 35.6 ng L^{-1} , 16.2–54.3 ng L^{-1} , and 41.8–135.3 ng L^{-1} , respectively, following the reduction in current to 1 A whereas their concentration was decreasing at 1.7 A (Fig. S3). This is consistent with past studies claiming that electrochemical oxidation is very efficient towards PFOS, but not PFOA for which Advanced Oxidation/reduction Processes (AOP/ARP) activated with UV, ultrasound or ionizing radiation show much higher degradation efficiencies (Leung et al., 2022). This suggests that sequential process of electrochemical oxidation and AOP/ARP could provide a better solution.

Ignoring the energy required for mixing and adsorption, the energy associated with the electrochemical oxidation of PFOS equates to 1.95 and 7.8 kWh m^{-3} water treated for 10 and 40 min treatment time, respectively, which is significantly less than other technologies such as ultrasonication which required 1475 kWh m^{-3} water treated (Sharma et al., 2022). Moreover, this process does not require high temperature, pressure and harsh chemicals, but is efficient due to the in situ production of hydroxyl radicals. However, the degradation is much more efficient at low pH which is consistent with past electrochemical oxidation studies (Leung et al., 2022).

4. Conclusions

This research showed that PFOS could be adsorbed rapidly onto GIC (within 20 min), but only 42–68% could be removed by adsorption only. The adsorption followed a second order kinetics and the adsorption isotherm followed a Langmuir model with a maximum adsorption capacity of 54 $\mu\text{g g}^{-1}$. Once adsorbed onto GIC, PFOS did not desorb significantly and was readily broken down following a first order kinetics ($k = 0.0468 \text{ min}^{-1}$ and $t_{1/2} = 15 \text{ min}$), achieving 99% removal down to 130 ng L^{-1} using a current of 0.5 A after 5 cycles of 20 min adsorption followed by 10 min of electrochemical oxidation. Breakdown by-products included short chain perfluoroalkane sulfonates such as PFHpS, PFHxS, PFPeS, PFBS, but also perfluorocarboxylic acids such as PFOA, PFHxA and PFBA suggesting two independent degradation pathways. PFHpS, PFHxS, PFPeS, PFBS and PFOA could be broken down following a first order kinetics but required a higher current of 1.7 A achieving 93.5%, 85.7%, 71.2%, 74.7% and 71% removal, respectively. The values of the relative rate constant (k) depended upon chain length $k_{\text{PFHpS}} (4.32 \times 10^{-2} \text{ min}^{-1}; \text{corresponding half-life } 16 \text{ min}) \approx 2.1k_{\text{PFHxS}} \approx 3k_{\text{PFPeS}} \approx 3.8k_{\text{PFBS}} \approx 3.1k_{\text{PFOA}}$. The process shows promising results for the rapid removal of PFOS from $\mu\text{g L}^{-1}$ levels to less than 100 ng L^{-1} levels in 10 min using less than 2 kWh m^{-3} water treated, but further

research is needed for the complete removal of short chain by-products. Cheap and conductive adsorbent with higher adsorption capacity, higher constant current or longer regeneration time will be needed to remove completely the residual by-products present at the ng L^{-1} range following PFOS breakdown.

Funding

The authors thank the Japan Society for the Promotion of Science (JSPS) for a long-term invitational fellowship awarded to Dr Antoine Trzcinski (fellowship ID L21554).

Author contribution

Antoine Trzcinski: Experiments using the novel reactor, sampling and extraction, manuscript drafting. Kouji Harada: Analysis of samples using GC-MS, troubleshooting, calibration and revision of manuscript

Declaration of competing interest

The authors declare the following financial interests/personal relationships which may be considered as potential competing interests: Antoine Trzcinski reports financial support was provided by Japan Society for the Promotion of Science.

Data availability

No data was used for the research described in the article.

Appendix A. Supplementary data

Supplementary data to this article can be found online at <https://doi.org/10.1016/j.chemosphere.2023.138268>.

References

- Ambaye, T.G., Vaccari, M., Prasad, S., Rtimi, S., 2022. Recent progress and challenges on the removal of per- and poly-fluoroalkyl substances (PFAS) from contaminated soil and water. *Environ. Sci. Pollut. Res.* 29, 58405–58428.
- Asghar, H.M.A., Roberts, E.P.L., Hussain, S.N., Campen, A.K., Brown, N.W., 2012. Wastewater treatment by adsorption with electrochemical regeneration using graphite-based adsorbents. *J. Appl. Electrochem.* 42, 797–807.
- Bentel, M.J., Yu, Y., Xu, L., Li, Z., Wong, B.M., Men, Y., Liu, J., 2019. Defluorination of per- and polyfluoroalkyl substances (PFASs) with hydrated electrons: structural dependence and implications to PFAS remediation and management. *Environ. Sci. Technol.* 53, 3718–3728.
- Brown, N.W., Roberts, E.P.L., Chasiotis, A., Cherdrone, T., Sanghrajka, N., 2004. Atrazine removal using adsorption and electrochemical regeneration. *Water Res.* 38, 3067–3074.
- Carter, K.E., Farrell, J., 2008. Oxidative destruction of perfluorooctane sulfonate using boron-doped diamond film electrodes. *Environ. Sci. Technol.* 42, 6111–6115.
- Cheng, J., Vecitis, C.D., Park, H., Mader, B.T., Hoffmann, M.R., 2008. Sonochemical degradation of perfluorooctane sulfonate (PFOS) and perfluorooctanoate (PFOA) in landfill groundwater: environmental matrix effects. *Environ. Sci. Technol.* 42, 8057–8063.
- Dadashi Firouzjaei, M., Zolghadr, E., Ahmadi, S., Taghvaei, N., Akbari Afkhami, F., Nejati, S., Elliott, M.A., 2022. Chemistry, abundance, detection and treatment of per- and polyfluoroalkyl substances in water: a review. *Environ. Chem. Lett.* 20, 661–679.
- Deng, Y., Liang, Z., Lu, X., Chen, D., Li, Z., Wang, F., 2021. The degradation mechanisms of perfluorooctanoic acid (PFOA) and perfluorooctane sulfonic acid (PFOS) by different chemical methods: a critical review. *Chemosphere* 283, 131168.
- Du, Z., Deng, S., Bei, Y., Huang, Q., Wang, B., Huang, J., Yu, G., 2014. Adsorption behavior and mechanism of perfluorinated compounds on various adsorbents—a review. *J. Hazard Mater.* 274, 443–454.
- Du, Z., Deng, S., Chen, Y., Wang, B., Huang, J., Wang, Y., Yu, G., 2015. Removal of perfluorinated carboxylates from washing wastewater of perfluorooctanesulfonyl fluoride using activated carbons and resins. *J. Hazard Mater.* 286, 136–143.
- Elanchezhian, S.S., Preethi, J., Rathinam, K., Njaramba, L.K., Park, C.M., 2021. Synthesis of magnetic chitosan biopolymeric spheres and their adsorption performances for PFOA and PFOS from aqueous environment. *Carbohydr. Polym.* 267, 118165.
- EPA, U., 2016. Drinking Water Health Advisory for Perfluorooctane Sulfonate (PFOS). Office of Water (4304T). Health and Ecological Criteria Division EPA.

- Flores, N., Sharif, F., Yasri, N., Brillas, E., Sirés, I., Roberts, E.P.L., 2018. Removal of tyrosol from water by adsorption on carbonaceous materials and electrochemical advanced oxidation processes. *Chemosphere* 201, 807–815.
- Gu, Y., Dong, W., Luo, C., Liu, T., 2016. Efficient reductive decomposition of perfluorooctanesulfonate in a high photon flux UV/sulfite system. *Environ. Sci. Technol.* 50, 10554–10561.
- Hao, S., Choi, Y.-J., Wu, B., Higgins, C.P., Deeb, R., Strathmann, T.J., 2021. Hydrothermal alkaline treatment for destruction of per- and polyfluoroalkyl substances in aqueous film-forming foam. *Environ. Sci. Technol.* 55, 3283–3295.
- Harada, K.H., Fujii, Y., Zhu, J., Zheng, B., Cao, Y., Hitomi, T., 2020. Analysis of perfluorooctanesulfonate isomers and other perfluorinated alkyl acids in serum by in-port arylation gas chromatography negative chemical ionization-mass spectrometry. *Environ. Sci. Technol. Lett.* 7, 259–265.
- Hassan, M., Du, J., Liu, Y., Naidu, R., Zhang, J., Ahsan, M.A., Qi, F., 2022. Magnetic biochar for removal of perfluorooctane sulfonate (PFOS): interfacial interaction and adsorption mechanism. *Environ. Technol. Innovat.* 28, 102593.
- Hassan, M., Liu, Y., Naidu, R., Du, J., Qi, F., 2020. Adsorption of perfluorooctane sulfonate (PFOS) onto metal oxides modified biochar. *Environ. Technol. Innovat.* 19, 100816.
- Hussain, S.N., Asghar, H.M.A., Sattar, H., Brown, N.W., Roberts, E.P.L., 2015. Removal of tartrazine from water by adsorption with electrochemical regeneration. *Chem. Eng. Commun.* 202, 1280–1288.
- Hussain, S.N., Roberts, E.P.L., Asghar, H.M.A., Campen, A.K., Brown, N.W., 2013. Oxidation of phenol and the adsorption of breakdown products using a graphite adsorbent with electrochemical regeneration. *Electrochim. Acta* 92, 20–30.
- Hussain, S.N., Trzcinski, A.P., Asghar, H.M.A., Sattar, H., Brown, N.W., Roberts, E.P.L., 2016a. Disinfection performance of adsorption using graphite adsorbent coupled with electrochemical regeneration for various microorganisms present in water. *J. Ind. Eng. Chem.* 44, 216–225.
- Hussain, S.N., Trzcinski, A.P., Asghar, H.M.A., Sattar, H., Brown, N.W., Roberts, E.P.L., 2016b. Disinfection performance of adsorption using graphite adsorbent coupled with electrochemical regeneration for various microorganisms present in water. *J. Ind. Eng. Chem.* 44, 216–225.
- Kothawala, D.N., Köhler, S.J., Östlund, A., Wiberg, K., Ahrens, L., 2017. Influence of dissolved organic matter concentration and composition on the removal efficiency of perfluoroalkyl substances (PFASs) during drinking water treatment. *Water Res.* 121, 320–328.
- Kowald, C., Brorman, E., Shankar, S., Klemashevich, C., Staack, D., Pillai, S.D., 2021. PFOA and PFOS breakdown in experimental sand, laboratory-grade water, investigation-derived groundwater and wastewater effluent samples at 50 kGy electron beam dose. *Radiat. Phys. Chem.* 180, 109323.
- Leung, S.C.E., Shukla, P., Chen, D., Eftekhari, E., An, H., Zare, F., Ghasemi, N., Zhang, D., Nguyen, N.-T., Li, Q., 2022. Emerging technologies for PFOS/PFOA degradation and removal: a review. *Sci. Total Environ.* 827, 153669.
- Li, X., Chen, S., Quan, X., Zhang, Y., 2011. Enhanced adsorption of PFOA and PFOS on multiwalled carbon nanotubes under electrochemical assistance. *Environ. Sci. Technol.* 45, 8498–8505.
- Liao, Z., Farrell, J., 2009. Electrochemical oxidation of perfluorobutane sulfonate using boron-doped diamond film electrodes. *J. Appl. Electrochem.* 39, 1993–1999.
- Mohammed, F.M., Roberts, E.P., Campen, A.K., Brown, N.W., 2012. Wastewater treatment by multi-stage batch adsorption and electrochemical regeneration. *J. Electrochem. Sci. Eng.* 2, 223–236.
- Mohammed, F.M., Roberts, E.P.L., Hill, A., Campen, A.K., Brown, N.W., 2011. Continuous water treatment by adsorption and electrochemical regeneration. *Water Res.* 45, 3065–3074.
- NHMRC, 2022. NHMRC PFAS Guidance for Recreational Water - Frequently Asked Questions.
- Niu, J., Lin, H., Gong, C., Sun, X., 2013. Theoretical and experimental insights into the electrochemical mineralization mechanism of perfluorooctanoic acid. *Environ. Sci. Technol.* 47, 14341–14349.
- Niu, J., Lin, H., Xu, J., Wu, H., Li, Y., 2012. Electrochemical mineralization of perfluorocarboxylic acids (PFCAs) by Ce-doped modified porous nanocrystalline PbO₂ film electrode. *Environ. Sci. Technol.* 46, 10191–10198.
- Oki, R., 2015. Evaluation of the Use of a Graphite Intercalation Compound for the Development of a Grey Water Recycling System by Adsorption and Electrochemical Regeneration. School of Computing, Science and Engineering, College of Science and Technology, University of Salford, Salford, UK.
- Pinkard, B.R., Shetty, S., Stritzinger, D., Bellona, C., Novoselov, I.V., 2021. Destruction of perfluorooctanesulfonate (PFOS) in a batch supercritical water oxidation reactor. *Chemosphere* 279, 130834.
- Rodriguez-Freire, L., Balachandran, R., Sierra-Alvarez, R., Keswani, M., 2015. Effect of sound frequency and initial concentration on the sonochemical degradation of perfluorooctane sulfonate (PFOS). *J. Hazard Mater.* 300, 662–669.
- Senevirathna, S.T.M.L.D., Tanaka, S., Fujii, S., Kunacheva, C., Harada, H., Shivakoti, B. R., Okamoto, R., 2010. A comparative study of adsorption of perfluorooctane sulfonate (PFOS) onto granular activated carbon, ion-exchange polymers and non-ion-exchange polymers. *Chemosphere* 80, 647–651.
- Sharma, S., Shetti, N.P., Basu, S., Nadagouda, M.N., Aminabhavi, T.M., 2022. Remediation of per- and polyfluoroalkyls (PFAS) via electrochemical methods. *Chem. Eng. J.* 430, 132895.
- Singh, R.K., Brown, E., Thagard, S.M., Holsen, T.M., 2021. Treatment of PFAS-containing landfill leachate using an enhanced contact plasma reactor. *J. Hazard Mater.* 408, 124452.
- Singh, R.K., Fernando, S., Baygi, S.F., Multari, N., Thagard, S.M., Holsen, T.M., 2019. Breakdown products from perfluorinated alkyl substances (PFAS) degradation in a plasma-based water treatment process. *Environ. Sci. Technol.* 53, 2731–2738.
- Stoiber, T., Evans, S., Temkin, A.M., Andrews, D.Q., Naidenko, O.V., 2020. PFAS in drinking water: an emergent water quality threat. *Water Sol* 1, e49.
- Szabo, J., Hall, J., Magnuson, M., Panguluri, S., Meiners, G., 2017. Treatment of perfluorinated alkyl substances in wash water using granular activated carbon and mixed media. In: Washington, D. (Ed.), US EPA Report. EPA/600/R-17/175, 2017.
- Tang, C.Y., Fu, Q.S., Robertson, A.P., Criddle, C.S., Leckie, J.O., 2006. Use of reverse osmosis membranes to remove perfluorooctane sulfonate (PFOS) from semiconductor wastewater. *Environ. Sci. Technol.* 40, 7343–7349.
- Thompson, J., Eaglesham, G., Mueller, J., 2011. Concentrations of PFOS, PFOA and other perfluorinated alkyl acids in Australian drinking water. *Chemosphere* 83, 1320–1325.
- Trzcinski, A.P., Ofogebu, N., Stuckey, D.C., 2011. Post-treatment of the permeate of a submerged anaerobic membrane bioreactor (SMBR) treating landfill leachate. *J. Env. Sci. Health, Part A* 46, 1539–1548.
- Vecitis, C.D., Park, H., Cheng, J., Mader, B.T., Hoffmann, M.R., 2009. Treatment technologies for aqueous perfluorooctanesulfonate (PFOS) and perfluorooctanoate (PFOA). *Front. Environ. Sci. Eng. China* 3, 129–151.
- Zhang, C., Jiang, Y., Li, Y., Hu, Z., Zhou, L., Zhou, M., 2013. Three-dimensional electrochemical process for wastewater treatment: a general review. *Chem. Eng. J.* 228, 455–467.
- Zhang, D., He, Q., Wang, M., Zhang, W., Liang, Y., 2021. Sorption of perfluoroalkylated substances (PFASs) onto granular activated carbon and biochar. *Environ. Technol.* 42, 1798–1809.